JOURNAL OF SPACECRAFT AND ROCKETS
Vol. 46, No. 2, March–April 2009

Novel Sensor for Fast Heat-Flux Measurements

Helmut Knauss* and Tim Roediger†
University of Stuttgart, 70569 Stuttgart, Germany
Dimitry A. Bountin,‡ Boris V. Smorodsky,§ and Anatoly A. Maslov¶
Russian Academy of Sciences, 630090 Novosibirsk, Russia
and
Julio Srulijes**
French–German Research Institute of Saint-Louis, 68301 Saint-Louis Cedex, France

DOI: 10.2514/1.32011

The Atomic Layer Thermopile is a novel fast-response sensor for transient heat-flux measurements. The sensor's very fast frequency response allows for highly-time-resolved heat-flux measurements up to the 1 MHz range. Its working principle is based on the transverse Seebeck effect. The output signal is directly proportional to heat-flux density and has a linear characteristic from the $\mathrm{mW/cm^2}$ to the $\mathrm{kW/cm}$ range. Its steady and unsteady responses have been determined experimentally by a step change of imposed radiative flux. The results correlate well with theoretical values obtained from analytical solutions. Furthermore, the dynamic properties of the Atomic Layer Thermopile have also been evaluated by a passing shock wave. The Atomic Layer Thermopile gauge recorded a steplike change in heat flux less than 1 μs after the shock had passed. After the peak heat flux, a laminar boundary-layer state could be detected for a unit Reynolds number of 11.31×10^6/m. In addition, in particular, the temporal resolution and the spatial resolution of the Atomic Layer Thermopile were demonstrated in instability studies performed in a hypersonic conical boundary layer at $M = 6$. In addition to second-mode instability in the 220–370 kHz frequency range, a second peak in the spectra revealed a first harmonic of this instability at 430–730 kHz.

Nomenclature

A	=	amplitude or mass-flux disturbance
a	=	thermal diffusivity
a_{ref}	=	reference area
C	=	heat capacity in Eq. (5)
c_p	=	specific heat at constant pressure
d	=	oxygen concentration
$\bar{E}$	=	thermoelectric field
f	=	frequency
i	=	intensity
k	=	thermal conductivity
L	=	linear Lees–Lin operator
l	=	film length
M	=	Mach number
P	=	pressure
P_{laser}	=	laser power
Pr	=	Prandtl number
p	=	pressure disturbance
q	=	heat-flux density
R	=	ohmic resistance
R_{CS}	=	thermal contact surface resistance between the film and substrate
R_F	=	thermal resistance of the film
Re	=	Reynolds number
Re_{unit}	=	unit Reynolds number
$\underline{r}(0)$	=	recovery factor
$\bar{S}$	=	Seebeck tensor
St	=	Stanton number
s	=	sensitivity coefficient
$s'(0)$	=	functions of the boundary-layer velocity profiles in Eq. (7)
T	=	temperature
U	=	velocity or voltage
u, v, w	=	streamwise, wall normal, and spanwise disturbance velocity components
x	=	distance from the shock that a particle travels in the freestream relative to the wall ($u_2 t$)
x_p	=	distance from the shock traveled by a particle because of initially being set in motion by the shock $[U_2 U_s t/(U_s - U_2)]$
x^*	=	distance along the generic line of the cone
α, β	=	streamwise and spanwise wave numbers
α_a	=	absorption coefficient
α_c	=	tilt angle
Γ	=	density ratio across the shock
γ	=	ratio of specific heat capacities
δ	=	thickness
θ	=	nondimensional temperature disturbance
ϑ	=	semicone angle
κ	=	wall-temperature gradient induced by the instability wave
λ	=	wave length
μ	=	dynamic viscosity
ρ	=	density or density disturbance
τ	=	time constant
χ	=	angle between the wave vector and mean flow direction in the tangential plane of the model surface

Presented as Paper 3637 at the 25th AIAA Aerodynamic Measurement Technology and Ground Testing Conference, San Francisco, CA, 5–8 June 2006; received 7 May 2007; accepted for publication 11 August 2008.

*Senior Scientist, Institute of Aerodynamics and Gas Dynamics, Pfaffenwaldring 21. Member AIAA, Retired.
†Research Engineer, Doctoral Student, Institute of Aerodynamics and Gas Dynamics.
‡Junior Scientist, Institute of Theoretical and Applied Mechanics, Siberian Branch, Hypersonic Flow Laboratory.
§Senior Scientist, Institute of Theoretical and Applied Mechanics, Siberian Branch, Laboratory of Wave Processes.
¶Professor, Deputy Director, Institute of Theoretical and Applied Mechanics, Siberian Branch, Head of Hypersonic Flow Laboratory. Member AIAA.
**Senior Scientist.

ψ = shock wave angle
ω = nondimensional frequency

Subscripts

ALTP = Atomic Layer Thermopile
a = absorption
B = Blasius length scale
c = coated sensor
e = boundary-layer edge conditions
F = Atomic Layer Thermopile film
f = Fourier amplitude
ind = induced in calibration
L = laminar boundary layer
m = measured
max = maximum
n = normal to surface
p = particle distance because of initially being set in motion by the shock
r = recovery factor
S = Atomic Layer Thermopile substrate
s = shock properties
T = total
t = transition
trans = translatory mode
uc = uncoated sensor
w = conditions at the wall
0 = initial
1 = initial condition in front of the shock wave
2 = condition behind the shock wave outside of the boundary layer

I. Introduction

THE past few years have witnessed a growing interest in the measurement of unsteady heat transfer phenomena. This increase in interest is due to the need and desire to understand the heat transfer process that occurs in inherently unsteady environments and to support the numerical modeling of unsteady heat transfer phenomena in suitable validating experiments. Research has been conducted on a number of topics involving both natural and forced unsteadiness, including turbine blade heat transfer, boundary-layer transition, turbulent boundary layer, etc.

Despite the vast progress made in the field of optical measurement techniques for determining global heat-flux distribution on the surface using various methods, including the liquid crystal technique, infrared and phosphor thermography, and temperature-sensitive paint, there is still an urgent need for a single-point heat transfer measurement technique of high temporal resolution. This is primarily due to the lack of temporal resolution of all optical methods to capture real high-frequency fluctuations of heat flux at the wall. Situations such as these might occur in conjunction with flow phenomena that are present in the transitional process of a hypersonic boundary layer from the very beginning of transition till downstream to the turbulent state. In such a high-speed flow, two gauge parameters are therefore of importance: the gauge sensitivity (voltage output and heat-flux density) and the time response should be as high as possible to achieve a large signal/noise ratio even at high frequencies.

A wide range of well-established single-point heat-flux gauges is available for various applications in thermodynamics and fluid mechanics with different characteristics. Conventional gauges may be categorized as gauges based on the following: 1) the dissipation of electric power from a heater mounted on the substrate surface, 2) transient surface-temperature measurement using various techniques such as those involving coaxial thermocouples and thin-film assistance elements, and 3) temperature-difference measurements that include the well-established Gardon-type gauges, Schmidt–Boelter gauges, and standard layered gauges, which have achieved a very high level of perfection and performance in the form of microsensors.

The gauges listed previously are ordered by decreasing time constant (i.e., increasing frequency response). An overview of the heat-flux sensors of these categories with regard to criteria such as time response, its definition and determination, as well as other sensor-specific features, is provided by Knauss et al [1], along with an extensive list of references.

This paper aims at demonstrating the characteristics of a new heat-flux gauge as an example of a new category of heat-flux gauges. The new category 4 gauges are basically a logical continuation of the layered microsensors in category 3. By means of the transverse Seebeck effect (TSE), it is possible to realize a sensor with a thickness of 10–100 nm in only one thin-film unit. The TSE is caused by an anisotropy of the film in conjunction with the tilt angle of the crystal with respect to the film-surface normal. The TSE was already theoretically predicted in 1941, but was probably only first made usable in yttrium–barium–copper–oxide ($YBa_2Cu_3O_{3-d}$ = YBCO) films [2–4]. Such active films are the basis for the current patented sensor, known as the Atomic Layer Thermopile (ALTP) and manufactured by FORTECH. Its anisotropic structure is formed by a sequence of well-conducting layers and layers that are more insulating, leading to a thermopile that consists of thermocouples of atomic dimensions connected in series. In laboratory tests on very thin YBCO films ($\delta_F \approx$ several tens of nanometers), a bandwidth up to about 1 GHz could be achieved [3]. Another advantage is that the sensor does not require active heating of the film. The ALTP is a wall-isothermal sensor and does not produce thermal disturbances such as hot wires or films. It is therefore very suitable for an array arrangement without thermal interference.

In addition to the ALTP, two other heat-flux gauges based on the TSE are documented in literature. The first alternative was presented by Mityakov et al. [5] in 2002. Their gradient heat-flux sensor (GHFS) is based on the use of anisotropic pure-bismuth single crystals. The GHFS operates in a heat-flux density range from mW/cm^2 to some hundred W/cm^2, as shown by Sapozhnikov et al. [6]. The time constant of 50 μs specified by the authors contradicts, to some extent, the heat-flux time history resulting from the passage of the incident shock according to Fig. 1 in [6].

The second alternative follows the principle presented by Zahner et al. [7]. Instead of tilted crystal structures, tilted multiple metallic layers made of copper/constantan were used. Zahner et al. predicted that the time constants for these films could be lowered from the millisecond to the microsecond range for a reduction of film thickness in the range of 10 μm. Based on this principle, Raphael-Mabel [8] conducted fundamental research with a combination of steel and brass for a high-temperature heat-flux sensor in 2005. Both authors focused on heat-flux measurements for long periods of time in high-temperature and high-heat-flux environments. The ALTP, however, is primarily adapted to transient unsteady measurements and not to long-term measurements. The latter application is not excluded for this sensor: it has already been tested but shall not be discussed in this paper.

II. Atomic Layer Thermopile

A. Principle of Operation

As stated in the Introduction, the ALTP works on the principle of the TSE. The anisotropic YBCO film consists of copper-oxide layers with YBCO interlayers (see Fig. 1a). A thermoelectric field, directly proportional to the temperature gradient in the film, is induced in the direction of the film layer. The resulting thermoelectric voltage U produced by a temperature difference over the YBCO film due to the absorption of radiation or convective heat transfer is given by

$$U = \frac{l}{\delta_F} \Delta S \Delta T \frac{\sin 2\alpha_c}{2} \tag{1}$$

where l is the length of the film (normal to the layer orientation), the film thickness , the temperature difference between the front and rear sides of the film (see Fig. 1a), and $\Delta S = (S_c - S_{ab})$ is the difference in the thermo power values of the Seebeck tensor $\bar{\bar{S}}$ defined for the

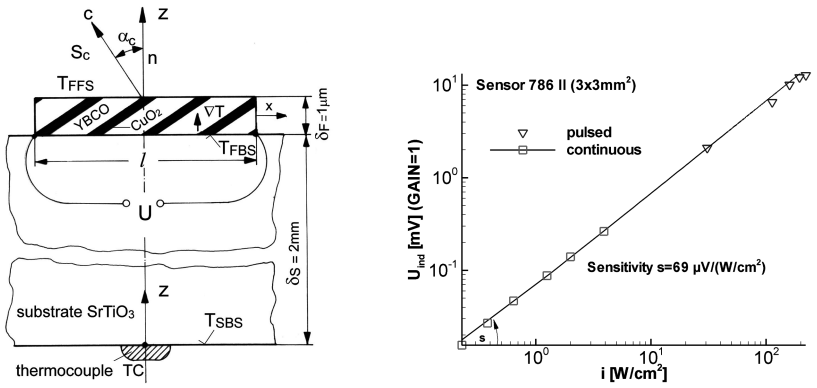

a) b)

Fig. 1 Structure and characteristics of the ALTP: a) schematic cross section of a tilted YBCO film (FFS indicates the front side, and FBS and SBS indicate the rear side of the film and the substrate, respectively) and b) calibration curve for continuous and pulsed laser sources.

untilted crystal (normal and parallel to the c axis). Equation (1) is derived in detail in [9].

1. Static Calibration

Laser calibration experiments have shown a linear characteristic of the sensor over more than 11 orders of magnitude. Heat-flux rates of a few mW/cm^2 up to 2×10^3 W/cm^2 (damage threshold for a 1 ms pulse) can be detected with the ALTP. The static calibration is carried out with the intention of assigning the absorbed part of a parallel CO_2 laser beam of known intensity on the ALTP film surface to a measured heat-flux density. The sensor is totally exposed to an incident radiation of known intensity i. For a detailed description of the setup and static calibration procedure, the reader is referred to [9,10]. A resulting calibration curve (gain=1) with a logarithmic scale on both axes of an ALTP after exposure to a dc-excited CO_2 laser for low intensities and a pulsed laser source for higher intensities is illustrated in Fig. 1b. The slope of the curve shows a typical ALTP sensitivity of $s = 69\ \mu\text{V}/(\text{W/cm}^2)$.

The total uncertainty of the calibration procedure can be estimated from the following equation defining the sensitivity coefficient:

$$s = \frac{U_{\text{ind}}}{\alpha_a i} \tag{2}$$

where α_a is the absorption coefficient of the sensor surface. By differentiating this expression and adding the rms values of all single uncertainties, we have an overall uncertainty in the calibration of about 5.5%.

The sensitivity of uncoated ALTP sensors decreases with time due to the hygroscopic character of the YBCO films. For such sensors, a recalibration period of several months, depending on the test environment, is recommended for quantitative heat-flux measurements. The sensors without a coating, however, can be used for measurements of heat-flux fluctuations with very good spatial resolution and with high temporal resolution in particular. At present, sensors with a film thickness between 500–700 nm and an active area of 20.4 mm have been used successfully. The dynamic calibration as subsequently described further shows a temporal resolution up to 1 MHz.

To avoid the decrease in sensitivity of uncoated sensors, a protective coating was developed. The coating stabilizes the sensitivity of the sensor significantly but reduces the temporal resolution of the sensor to a certain degree (200–250 kHz).

2. Optical Properties of ALTP Film with and Without a Protective Coating

In addition to convective heat, the ALTP also captures incident radiation over a very large wavelength range from far infrared to ultraviolet. Strictly speaking, the induced signal in the active film is caused by a temperature gradient that either originates from absorbed radiation, convective heat transfer on the surface, or any superposition of these two modes of thermal energy. Separation of the two modes is only possible with knowledge of the prevailing emission conditions in the surrounding gas flow and the optical properties of the sensor surface with and without a protective coating.

The spectral response of (uncoated) YBCO films has been investigated in literature [11–13] and references therein. In the far infrared (0.8–400 μm), YBCO films possess a metal-like absorption and reach very low absorptivities: as far as $\sim$10%. In the visible region (400–800 nm), reduced absorption is witnessed (i.e., 50% at 500 nm). The absorption reaches nearly 100% for shorter wavelengths in the UV range (20–400 nm). The translation of these properties in terms of temperature concludes that at low temperatures (e.g., 300 K $\cong$ 10 μm according to Wien's Law, normal spectrum), the radiative contribution to the sensor signal is negligible. For high temperatures (5000 K $\cong$ 0.58 μm), the absorption increases to $\sim$50% and radiation ought to contribute considerably to the thermoelectric signal.

The major difference created by the protective coating is a sharp absorption peak of 86% at $\sim$10 μm, which is desirable for static calibration. In a 300 nm to $\sim$1 μm range, the coating can be considered as almost transparent and the optical properties are similar to the uncoated film. Thus, at low temperatures, the radiative contribution should still be very limited due to low emission intensities.

B. Dynamic Properties

Theoretical estimations for very thin films, studied by Zeuner et al. [14], have shown that the relevant time response depends on different parameters: namely, the film thickness, the tilting angle of the layers, the thermal contact surface resistance R_{CS} between film and substrate, the diffusivity of the film, the substrate material, and possibly the thickness of a protection coating. In films with a greater thickness such as $\delta_F = 250$–400 nm or higher, where $R_F \gg R_{\text{CS}}$, the diffusion time of the film dominates and the time constant is, as is typical in a diffusion process, proportional to the film thickness:

$$\tau \approx 0.4\delta_{F^2}/a \tag{3}$$

where a is the thermal diffusivity of the film. Equation (3) can be applied to obtain a rough estimate of the time constant of the actual uncoated ALTP films used in current investigations. A film thickness of $\delta_F \approx 700$ nm and a diffusivity value of about $a \approx 0.007$ cm^2/s yield a time constant of about $\tau \approx 0.3$ μs.

1. Experimental Investigation

To investigate the amplitude-frequency-response (AFR) characteristic more precisely, dynamic calibration has been carried out. The measuring unit consisting of a sensor and an amplifier was exposed to the radiation of a dc-excited CO_2 laser with a power of 25 mW. Because of such a low laser power, a custom-made amplifier (COSYTEC) of gain 5000 was used. The calibration setup is

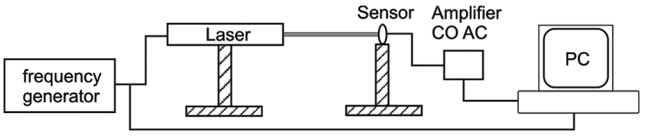

Fig. 2 Schematic setup of amplitude-frequency-response calibration (CO AC denotes the COSYTEC amplifier with high-pass filter).

illustrated schematically in Fig. 2. A frequency generator, producing a step function pulse (Fig. 3), excites the laser light pulse detected by the sensor.

By dividing the spectrum of the system output signal by the generated base signal spectrum and normalizing the result, AFR coefficients of the system are obtained (Fig. 4). The fast decrease of the coefficients found beyond 600 kHz is related to the time constant of the ALTP sensor itself, due to its film thickness, because the characteristic of the amplifier does not exhibit a −3 dB rolloff until 1 MHz. The difference in the ALTP frequency response (670I and 671I) beyond about 400 kHz (Fig. 4) is caused by a slightly different film thickness.

A time constant can be derived from Fig. 4 based on the equation

$$A = \frac{A_0}{\sqrt{1 + (2\pi f\tau)^2}} \tag{4}$$

where A is the Fourier amplitude and f the frequency. For a prescribed attenuation of -3 dB equivalent to $A/A_0 = 0.71$ according to the frequency response in Fig. 4, a frequency $f \approx$ 300 kHz can be assigned. For $2\pi ft = 1$ in Eq. (4), a time constant $\tau \approx 0.5$ μs can be deduced. This value is in the same range as the time constant estimated by relation (3). In comparison, the corresponding characteristics for common hot-wire probes used in Sec. IV is $0.1–1 \times 10^{-3}$ s.

2. *Theoretical Investigation*

To determine a theoretical (ideal, that is, without an amplifier) frequency response of the ALTP, it is necessary to solve a boundary-value problem for the one-dimensional equation of heat conduction in the solid body of the sensor. In this paper, we have used analytical solutions given by Carslaw and Jaeger [15] for time-periodic excitation at the surface

$$q(x = 0, t) = q_0 e^{-i2\pi ft} \tag{5}$$

where f is the frequency of a flat solid slab composed of several layers with different thermal properties. The frequency response is determined from the heat flux, spatially averaged through the sensitive layer normalized to the amplitude of the heat flux specified at the surface:

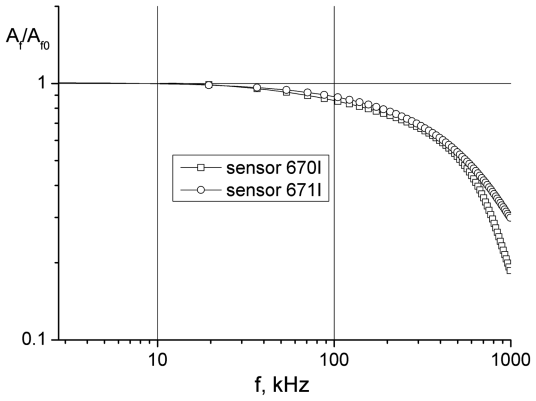

Fig. 4 Amplitude-frequency-response coefficients of the system (sensor and amplifier) for two ALTPs of slightly different film thicknesses.

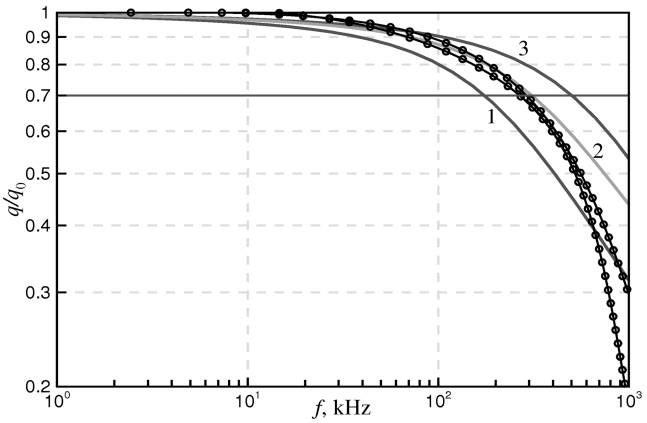

Fig. 5 Frequency response of ALTP sensors for normalized averaged heat flux $\langle q\rangle/q_0$ across the sensitive film versus frequency f. Comparison of measurement (see Fig. 4 for symbols) with theory (solid lines). Thickness of the sensitive film $\delta_F = 1$, 0.7, 0.6 μm for curves 1–3, respectively.

$$\langle q\rangle/q_0 = \Delta T_F/\delta_F q_0 \tag{6}$$

where ΔT_f is a temperature difference across the sensitive film. Figure 5 presents a comparison of the measured frequency response shown in Fig. 4 with such a computation for uncoated sensors, when varying the thickness of the sensitive film. The thickness of the substrate for relevant frequencies ($f \geq 1$ kHz) does not affect the result of the computations. For this reason, the substrate has been assumed to be a semi-infinite body. The measured frequency

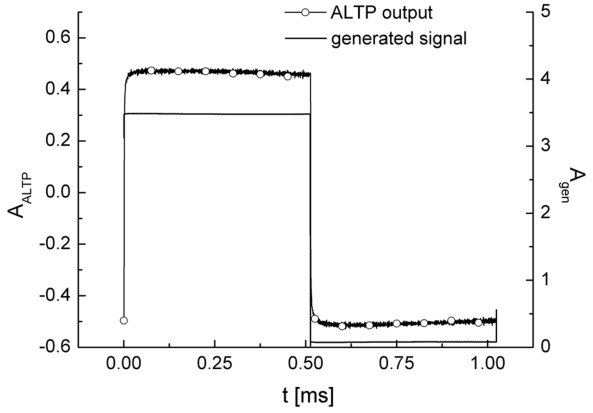

a)

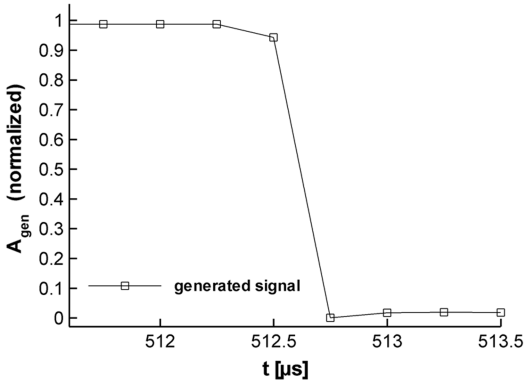

b)

Fig. 3 Plots of a) an example of a generated step function and sensor response (ALTP 670I) (amplitudes are in arbitrary units) and b) an enlargement of a generated reference step-rise signal generated by the diode laser (normalized to step height).

responses correlate best with the computational results when assuming $\delta_F = 0.7$ μm (curve 2 in Fig. 5), which corresponds to the specification given by FORTECH. It seems that this correlation is good for frequencies $f \leq 300$ kHz.

Comparing measured frequency-response curves with theoretical curves can also be an indirect means of estimating the thickness of the sensitive layer. The gain of frequency response beyond 300 kHz with decreasing film thickness from 1 to 0.6 μm is clearly seen by comparing curves 1 to 3 and shows the potential of a possible bandwidth enlargement into the megahertz range with thinner films.

III. Heat-Flux Measurements in a Shock-Tube Boundary Layer

The first objective of this investigation is to evaluate the dynamic response of the ALTP by its response to a steplike change in the convective heat flux by a passing shock wave. The shock wave creates a very sharp step rise in the convective heat flux at the wall in the same order of magnitude as that of the laser pulse (see Fig. 3b).

A second aim is to study the boundary layer (BL) formed behind the moving shock wave and compare the heat transfer measurements to previous theoretical and experimental investigations of the laminar, transitional and turbulent state of the BL.

A. Experimental Facility and Conditions

The experiments have been carried out in the ST70A French–German Research Institute of Saint-Louis (ISL) shock tube. The driver section is 2 m long and separated by a Mylar diaphragm from a driven section that is 6.5 m in length. The tube has an inner diameter of 70 mm with a honed surface to reduce its surface roughness. Connecting elements between the steel tube segments allow 6 sensors to be installed at a defined cross section of the tube. Comparative simultaneous measurements between commercial thin-film gauges produced by the Shock Wave Laboratory [16] and the ALTP with and without a protective coating have been carried out at a position 6 m downstream of the Mylar diaphragm and 0.5 m upstream of the tube end. The sensitivity of the ALTPs and the specification of the thin-film gauge are listed in Table 1.

Low-noise amplifiers (nominal gain of 100) have been used for the amplification of the ALTP sensor signals. All signals have been captured with a sampling rate of 40 MHz and 14-bit resolution.

The characteristics of the instationary boundary layer behind a moving shock and the time response of the ALTP have been studied and discussed for one model case. This test case has been reproduced several times with similar test conditions and showed a good repeatability of the temporal response signals. To generate a faster shock, helium has been used as a driver gas, which was separated by a 250 μm Mylar diaphragm from the driven section filled with N_2. An initial pressure $P_1 = 0.102$ bar was established in the low-pressure tube and the wall temperature was $T_w = 298.9$ K. The determined shock velocity $U_s = 1156$ m/s resulted in a shock Mach number of $M_s = 3.28$. The calculation of the conditions behind the shock outside of the BL, indicated by subscript 2, yielded a static temperature $T_2 = 881$ K, a velocity $U_2 = 880$ m/s, and a Mach number $M_2 = 1.43$. The density ratio across the shock,

$$\Gamma = \frac{U_s}{U_s - U_2} = \frac{\rho_2}{\rho_1} \tag{7}$$

is approximately 4.25.

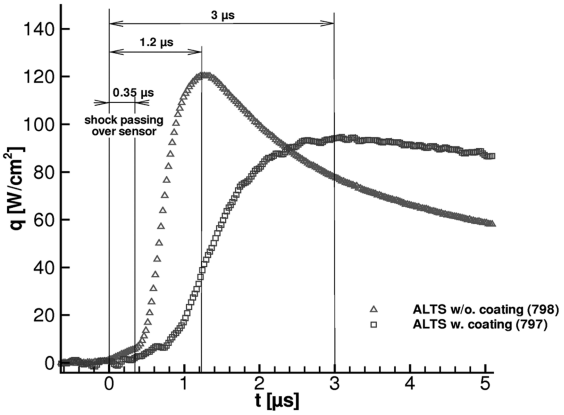

Fig. 6 Response of coated and uncoated ALTP to the incident shock wave.

B. Evaluation of the ALTP Dynamic Response by Means of a Passing Shock Wave

The evaluations of the dynamic properties and time response of wall-mounted sensors by a passing shock wave has several favorable characteristics:

1) The incident shock wave produces a steplike change in heat flux in a convection environment as well as in the emission characteristics of the prevailing gas.

2) The formation of the shock wave and the developing BL can be regarded mainly as two-dimensional assuming a fairly symmetric burst of the diaphragm. Thus, the response of different sensors arranged in one circumference of a tube cross section can be compared simultaneously.

3) The boundary conditions of the experiments are fairly repeatable and easy to measure.

A passing shock wave was used to investigate several gauges in the past [17–20].

Figure 6 shows a magnification of the response to the incident shock. The scale is plotted in microseconds and the data points are marked for a 40 MHz sampling rate (no filtering has been applied). The initial slope of the signal shows the shock passing over the sensor ($t < 0.35$ μs) before it significantly increases and the heat-flux reaches a maximum at $t = 1.2$ μs for the uncoated sensor and $t = 3$ μs for the coated sensor with peak values of 120 and 95 W/cm^2, respectively. The measured time of the shock passing corresponds exactly to the time that can be calculated from the shock speed U_s and the width of the sensor normal to the shock front (0.4 mm). The difference in the rising slope between the coated and uncoated sensor clearly shows the increase in response time due to coating. Nevertheless, the response time even of the coated sensor is lower than any other heat-flux gauge known to the authors.

The characteristic sharp rise of the signals can be deduced from the physical phenomena developing immediately behind the passing of the shock wave. On the one hand, the peak results from the very thin initial BL thickness behind the shock, causing a large temperature gradient at the wall and leading consequently to a considerable convective heat load. On the other hand, radiative processes immediately behind the shock front could lead to a radiative contribution in the thermoelectric signal, which is determined by the gas temperature T_2 behind the incident shock wave. In the present experiments, translatory and rotational degrees of freedom are excited as well as the rotational degrees to some extent because

Table 1 Specification of installed ALTP and thin-film gauges

Sensor (serial number)	Active area, mm^2	Sensitivity s (gain=1)	$\sqrt{\rho c k}$ of substrate, J/(cm^2 K$\sqrt{s}$)	Resistance Ω
ALTP without coating (798)	0.4 × 2	182 μV/(W/cm^2)	0.5246	125
ALTP with coating (797)	0.4 × 2	127 μV/(W/cm^2)	0.5246	291
Thin-film gauge (P-657)	0.3 × 0.9	3852 μV/(Ws$^{1/2}$/cm^2)	0.3223	28.67

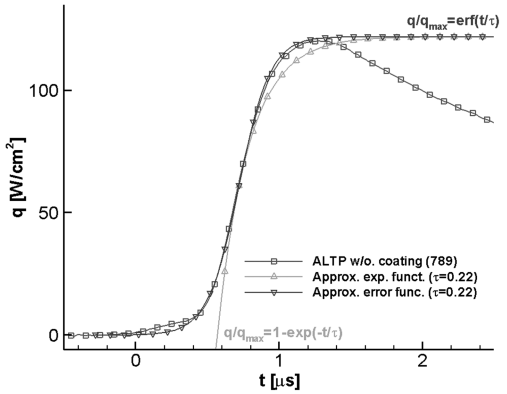

Fig. 7 Approximation of the response to the incident shock wave for the uncoated ALTP.

nitrogen was used as the driven gas. At $M_s = 3.28$, all three are practically in thermodynamic equilibrium, in which the translatory, the rotational and the vibrational temperatures are equal to T_2. Dissociation and ionization can be excluded for the moderate shock Mach number $M_s = 3.28$ with a low shock strength. One way to separate the radiative and convective components could be performed by simultaneous spectroscopic measurements in the shock BL. But obviously the radiative part compared with the total heat flux is very small and beyond the scope of this paper but could be the subject of future work dealing with higher Mach numbers.

The time constants of the coated and uncoated sensor can be estimated from the time history in Fig. 6. Holmberg et al. [18] characterized the response of their sensor from the numerical modeling as a first order exponential rise. Figure 7 shows, however, that an approximation by an error function seems to be more suitable,

$$\frac{q}{q_{\max}} = \operatorname{erf}\left(\frac{t}{\tau}\right) \tag{8}$$

leading to the same time constant of $\tau_{\mathrm{uc}} = 0.22\ \mu$s for the coated sensor and $\tau_c = 0.55\ \mu$s for the uncoated one. The time constants obtained are in the range as predicted from theory and dynamic laser calibration in Sec. III.B.

C. Investigation of the BL Forming Behind the Shock Wave

1. *Theory and Definitions*

A shock wave that travels into a stationary fluid bounded by a wall creates an instationary boundary layer along the wall. In a shock-fixed coordinate system, the BL which grows from the foot of the shock can be regarded as quasi-steady. It differs from the usual (stationary) BL in that in this coordinate system the wall moves with a velocity of the shock wave. The shear stress and heat transfer vary with distance from the leading edge in the same manner as in the stationary case. Mirels [21] found a solution for the *laminar BL* equations between the shock wave that moves into a stationary fluid over an infinite flat plate. An expression, based on Mirels's solution, for the heat transfer rate into the wall is given in [22]:

$$q = s'(0)(T_w - T_r)\frac{c_p}{Pr}\sqrt{\frac{\rho_w \mu_w (U_s - U_2)}{2U_s t}} \tag{9}$$

where T_w is the wall temperature, T_r is the recovery temperature defined by

$$T_r = T_2\left\{1 + r(0)\frac{\gamma - 1}{2}M_2^2\right\} \tag{10}$$

γ is the ratio of specific heat capacities, and M_2 the flow Mach number behind the shock. $r(0)$ and $s'(0)$ are functions of the BL velocity profiles and the subscript w wall conditions.

The solution shows that the heat flux at a fixed location x into the wall decreases with $t^{-1/2}$, where t is the time after the passing of the shock wave. Later Mirels [23] gave an interpolation formula for $r(0)$ and $s'(0)$ which closely fit his numerical results in the form of

$$s'(0) = 0.489\sqrt{1 + 1.664\Gamma}Pr^{0.48+0.022\Gamma} \tag{11}$$

and

$$r(0) = Pr^{0.39-0.023\Gamma} \tag{12}$$

where $\Gamma = U_s/(U_s - U_2)$, which is equivalent to the density ratio ρ_2/ρ_1 across the shock.

The transition from laminar to turbulent occurs within a certain time interval $t_{t,\mathrm{onset}}$ to $t_{t,\mathrm{end}}$. For a fixed location, the unsteady heat flux into the wall increases significantly during the transition process.

In a *turbulent BL*, Weatherstone et al. [24] and Mirels [25] estimated the heat flux for a fixed location to decrease proportionally to $t^{-1/5}$. Different power laws can be found in literature as well as different approximations for the heat-flux rate into the wall of a turbulent BL. A review of references concerning this subject is given by Oertel [26] before 1966 and by Spence and Woods [27] before 1964. Experimental studies of the laminar and turbulent boundary layer behind a moving shock and the transition process were carried out in various facilities by means of optical methods and wall-mounted probes in supersonic flows. An overview of transient surface temperature and heat-flux measurements before 1959 was given by Hartunian et al. [28]. Further experiments on shock-tube wall boundary-layer transition and comparisons with theoretical estimations can be found in [17,22,29–34]. It should be noted that the work of Davies and Bernstein [22] studied the shock-induced boundary layer on a semi-infinite flat plate. In a shock-fixed reference frame, however, the results can be compared with the present investigation as mentioned previously.

The common definition of the shock-tube Reynolds number, based on laboratory reference coordinates, is

$$Re = \frac{\rho_2 U_2 x}{\mu_2} = \frac{\rho_2 U_2^2 t}{\mu_2} \tag{13}$$

where μ_2 is obtained from Sutherland's law and the characteristic length x is the distance that a particle travels in the *freestream* relative to the wall in the time t. The unit Reynolds number for the selected test case was $Re_{\mathrm{unit}} \approx 11.31 \times 10^6/\mathrm{m}$. The Stanton number is defined by

$$St = \frac{q}{\rho_2 U_2 c_{p,2}(T_r - T_w)} \tag{14}$$

where q is the heat-flux density, T_r is the recovery temperature as defined in Eq. (10), and c_p the specific heat at constant pressure.

2. *Experimental Results*

Figure 8 shows the signal response of the two ALTP sensors and the thin-film gauge to the shock passage, representing the time history of the instationary boundary-layer formation during the total measurement time of about 1.5 ms. According to Fig. 8, after the establishing phase of approximately 100 μs, due to the different response time of the three sensors, all sensor readings correlate well in the measured wall heat flux. The heat-flux signal of the thin-film gauge is superimposed by a digital noise because this heat-flux history has to be reconstructed out of the temperature time trace by applying the Cook and Felderman algorithm [35]. The signals of both ALTP sensors show a highly-resolved time history compared with the thin-film gauge. The scattering of the measured mean heat fluxes lies within 15%. The discrepancies in the mean values and the fluctuations of the time history could be caused by possible nonuniformities in the shock front and the preceding flow due to a slight asymmetric burst of the diaphragm, which violate the assumption of two-dimensional tube flow.

According to Mirels's theory, the heat flux of a laminar boundary layer at a fixed location x into the wall decreases with $t^{-1/2}$, thus the laminar region can be identified by the criterion $St\sqrt{Re} = \text{constant}$. The *constant* depends on the shock strength. Figure 9 shows a section

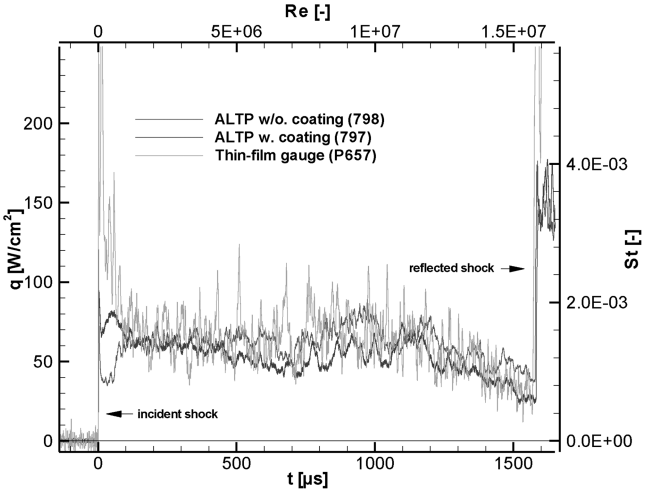

Fig. 8 Signal response of the ALTP with and without a coating compared with a thin-film gauge mounted in the same cross section (run 20050701-01).

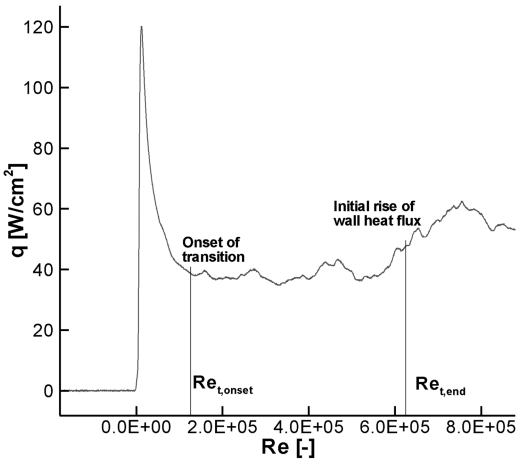

Fig. 10 Record of uncoated ALTP signal for revealing the laminar boundary layer, the onset of transition and delayed increase of wall heat flux.

of the expanded time history, which follows this law, identified by a constant plateau. The uncoated ALTP clearly exhibits a constant region immediately behind the heat-flux peak indicating shock passing. The coated sensor, however, does not reach a plateau like the uncoated one due to its larger time constant. Nevertheless, the slope of the signal decreases in the marked laminar region similar to the uncoated sensor. Consequently, according to the time history of the uncoated sensor, in the time interval $\Delta t_L = t_{L,\text{onset}} - t_{t,\text{onset}}$, a laminar boundary-layer state can be defined immediately behind the shock, with a calculated extension of about $\Delta x_l = u_2 \Delta t_l = 10$ mm.

The existence of a laminar boundary has already been shown experimentally for similar Mach numbers (e.g., in [22,28,34]), but has never been detected for such a high unit Reynolds number due to the confined time response of the gauges used in these experiments.

The determined value of the *constant* in the defined laminar region is approximately $St\sqrt{Re} \approx 0.29$. The *constant derived* from Mirels's theory using Eq. (9) and the interpolation formulas (11) and (12) results in $(St\sqrt{Re})_{\text{Mirels}} \approx 0.66$. Before any further studies at different shock strengths and unit Reynolds numbers are performed by means of high temporal resolved ALTP measurements, all explanations about the existing discrepancy between the present experimental results and Mirels's theory will be speculative.

The onset of a transition process is defined in which the trace deviates from the plateau and is marked in Fig. 9 with a corresponding postulated lowest transition Reynolds number $Re_{t,\text{onset}} \approx 1.25 \times 10^5$ according to the Reynolds number definition in Eq. (13). The time history in Fig. 10 shows, however, that the heat flux does not increase immediately from this point but the rise of heat flux is delayed for another 50 μs assigned to $Re_{t,\text{end}} \approx 6.25 \times 10^5$. A similar time history was observed by Davies and Bernstein [22] on a semi-infinite flat plate. The authors noted that as the boundary layer undergoes transition, the heating rate may continue to fall, but at a slower rate. The change in heat flux depends on the relative effectiveness of two opposing tendencies; the local thickening of the boundary layer reduces the wall heat flux, whereas the enhanced mixing tends to increase it. It was stated that a region might exist in which heat-flux density remains steady before rising as the turbulence level increases. This statement concurs with the time history found by the uncoated ALTP depicted in Fig. 10.

The definition of the transition Reynolds number (see Hartunian et al. [28] and Mirels [21]) differs from the Reynolds number defined in (13). The relevant characteristic length x_p, which describes the distance traveled by a particle because initially being set in motion by the shock and then reaching the transition point, is used as the characteristic distance for defining a transition Reynolds number, here indicated by subscript p:

$$Re_p = \frac{\rho_2 U_2 x_p}{\mu_2} = \frac{\rho_2 U_2^2}{\mu_2} \frac{U_s t}{(U_s - U_2)} \tag{15}$$

This Reynolds number should not be confused with the one given in Eq. (13). In the definition according to (15), a transition Reynolds number range $5.3 \times 10^5 \leq Re_{p,t} \leq 2.6 \times 10^6$ can be assigned. This interval concurs well with the BL transition correlation data presented by Hartunian et al. (Figure 2 in [28]) for the present shock strength $\Gamma = 4.25$ equivalent to $T_w/T_2 = 0.34$.

In the *turbulent boundary layer*, the heat flux decays with $t^{-1/5}$. Thus the time signal should evolve into a constant plateau for $StRe^{1/5} = \text{constant}$. Sometimes a one-seventh power law is more suitable for the transitional region and lower Mach numbers as already stated by Hartunian [28], but to consistently follow his assumption versus Re is plotted in Fig. 11. The *constant* again depends on the shock strength. Various theoretical and experimental values have been found by other authors and are added in Fig. 11 for comparison.

As we can see in the time history of the present investigation, the defined *constant* is slightly lower compared with the experimental value given by Hartunian [28] and Mirels's theoretical *constant* [25]. The actual numerical investigations carried out by the ISL (the

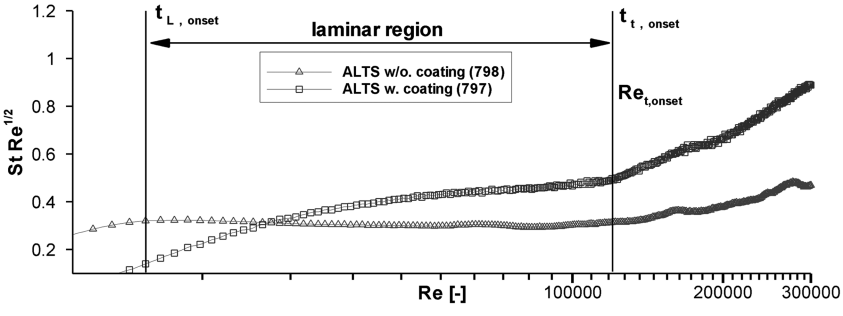

Fig. 9 Expansion of laminar boundary-layer time history measured by the ALTP sensors.

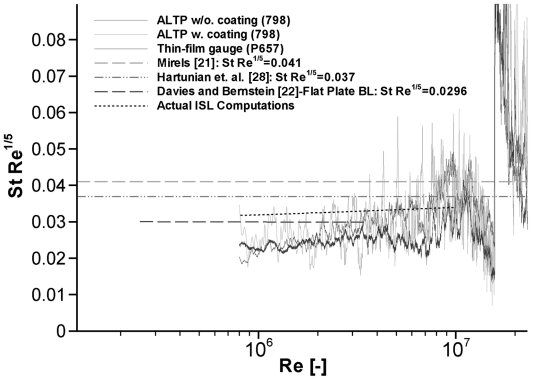

Fig. 11 Expansion and comparison of the turbulent boundary-layer time history with theoretical estimations by Mirels [25], experimental results published by Hartunian et al. [28], Davies and Bernstein [22], and actual computations carried out by ISL.

formulation of the implemented BL equations is described in [36]) show that a lower exponent for the power law is more suitable to describe the development of the turbulent BL and concurrence of the computed heat-flux densities with the experimental values is better with increasing time. These two features probably indicate that the turbulent boundary layer is not yet fully developed. In addition, the time trace of a thin-film gauge shows a behavior similar to the two ALTP sensors and independently confirms the ALTP measurements.

IV. Fluctuation Measurements in a Conical Boundary Layer at $M = 6$

Instability waves are known to play a major role in the laminar to turbulent transition process for boundary layers, at least for small initial wave amplitudes. For the subsonic and moderate supersonic flow regime, the most important ones are Tolmien-Schlichting waves, which find a continuation in the supersonic flow as the first instability mode (FM). For hypersonic velocities, another instability mode of an acoustical type leads to a turbulence breakdown-the second instability mode (SM). Mack was the first to identify these instability disturbances theoretically [37]. Experimentally, they were detected for the first time by Kendall [38], and later by Demetriades [39], Stetson et al. [40] and others. All stability data have been obtained by hot-wires so far. But the hot-wire anemometer technique has been limited to date, with the hot-wire probes available only achieving a bandwidth of $500 \div 600$ kHz, which does not seem to be sufficient for special studies in hypersonic boundary layers. On the other hand, this technique is restricted in its application in high-stagnation enthalpy flows because of inadequate overheat ratio and wire breakage. Therefore, it is very important to find other methods for stability investigations. The goal of the present experiment is to verify the possibility of the ALTP application for boundary-layer heat-flux fluctuation investigations. For this purpose, experiments in an unstable conical boundary layer were carried out and compared against hot-wire measurements obtained in the same tunnel and under the same conditions [41].

A. Experimental Setup

The experiments were carried out in the T-326 hypersonic wind tunnel of the Institute of Theoretical and Applied Mechanics, Siberian Branch of the Russian Academy of Sciences, at a Mach number of 5.95. The stagnation temperature was $T_0 = 400$ K, and the stagnation pressure was varied in the range $5.4–18.6 \times 10^5$ Pa, which yields unit Reynolds numbers $Re_{\text{unit}} = 6.4–20.9 \times 10^6$ m^{-1}. In all experiments, adiabatic wall conditions could be realized with an equilibrium temperature of about 330 K in the case of a laminar boundary layer. Thus, there was no mean heat flux to the model surface and ALTP sensors only measured instantaneous heat-flux fluctuations.

The model used was a 7 deg half-angle pointed steel cone (Fig. 12) with a length of 0.5 m. The constructive design of the cone body

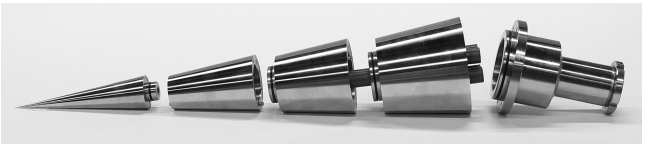

Fig. 12 Experimental model.

consists of 4 different segments. It allows the installation of up to 5 measuring units and up to 12 individual sensor-mounting locations in the cone surface. The model was installed under zero angle of attack with an accuracy of 0.2 deg. Two ALTP sensors were installed at the same station $x^* = 0.265$ m from the nose tip, at 90 deg to each other in the circumferential direction. The output signals were captured with a 12-bit A/D board at a sampling rate of 10 MHz. The averaged spectra (100 averages, 4096 samples) were smoothed by a running-average method. After smoothing, the noise was subtracted and spectral amplitudes were divided by the AFR coefficients, taking into account the AFR characteristic (see Fig. 4).

B. Results and Discussion

Figure 13 shows the spectra of sensor 670I for all regimes. The higher peaks in the plot correspond to the second mode (SM). It is located in different frequency ranges for different Reynolds numbers ($f \approx 220–370$ kHz) because of the SM properties. The second-mode wavelength is about twice the local boundary-layer thickness [40]. With an increasing unit Reynolds number, the boundary-layer thickness decreases and therefore leads to a higher SM frequency. Further peaks in the higher frequency range ($f \approx 430–730$ kHz) correspond to SM harmonics. In previous experiments carried out by means of a hot-wire (HW) probe in this tunnel, the SM harmonic was not detected because of a limited frequency range of the HWA system.

In the case of a local Reynolds number $Re = 7.21 \times 10^6$ and 7.19×10^6 assigned to the sensor positions, the SM amplitude is reduced and, at the same time, sufficient Fourier amplitudes increase in a wide frequency range (up to 900 kHz). This fact, as well as the disappearance of the harmonic in these regimes, is most likely due to the strong nonlinear processes already starting upstream of the gauge position. It shows that the BL is close to the turbulent state.

The derived ALTP spectra have been compared with hot-wire spectra obtained in previous experiments at the distance from the wall in which maximum fluctuations appear (Fig. 14). Each individual spectrum has been normalized by the maximum value of the second-mode Fourier amplitude. Good concurrence of values in the vicinity of the second-mode peak is clearly seen. The small discrepancy in SM frequency is due to a small deviation in the angle of attack between ALTP and HW cone experiments.

In the low-frequency range, Fourier amplitudes of the ALTP spectra are much lower compared with hot-wire spectra, and the local maximum corresponding to the first mode in the vicinity of 100 kHz is absent. The reason for such a big discrepancy had not been clear initially.

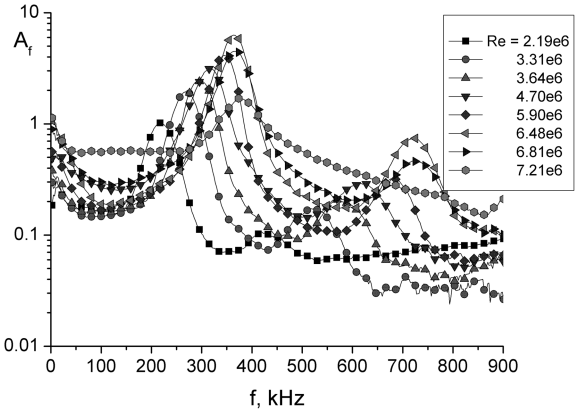

Fig. 13 Spectra of sensor 670I showing SM and its harmonics.

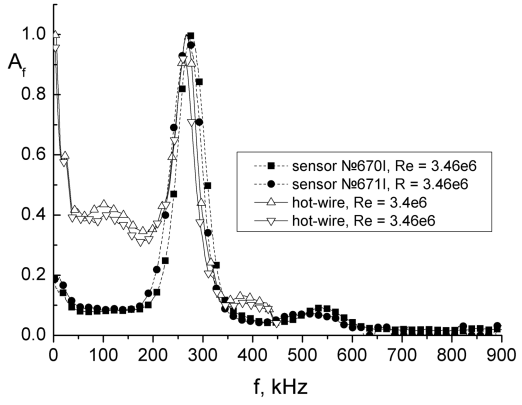

Fig. 14 Comparison of hot-wire and ALTP measurements.

To give a possible explanation for the observed discrepancy of the spectra measured by ALTP and HW in Fig. 14, the linear stability theory (LST) has been used in a theoretical investigation, which is described in great detail in [1]. In the following section, an abridged version of this study and its most relevant facts are given to substantiate this inconsistency.

The fluctuation of the wall heat flux measured by the ALTP sensor can be induced by the dominant disturbances in the unstable BL oscillations (instability waves) that have been detected. To determine the mean flow and the boundary conditions of the conical BL downstream of the shock wave attached to the sharp cone tip, the Taylor–Maccol equation [42] has been integrated numerically. For the 7 deg half-angle pointed cone with a freestream Mach number $M_1 = 5.9$, a Mach number $M_2 = 5.3$ behind the shock wave and a stagnation pressure ratio downstream/upstream of the shock $P_{0,2}/P_{0,1} = 0.9882$ resulted. M_2 has been defined as the Mach number at the BL outer edge. The reduced Mach number M_2 obtained and the stagnation pressure downstream of the oblique shock in the conical flow have been used to compute the self-similar cone boundary layer [43]. The viscosity has been based on Sutherland's law.

A linear stability analysis of this conical BL flow has been performed by numerical integration of the boundary-value problem for the Lees–Lin equations [44] by means of the method of orthonormalizations [45]. The streamwise wave number $\alpha = \alpha_r + i\alpha_i$, which can belong to the discrete or continuous spectrum, has been found as an eigenvalue of the problem, in which the imaginary part of the streamwise wave number α_i corresponds to the growth rate of the disturbance. LST computations have been performed for the actual ALTP sensor position at $x^* = 460$ mm and for stagnation conditions of the actual experiments (i.e., $T_0 = 390$ K and $P_0 = 10$ bar). More details of the computations can be found in [1].

These computations for the growth rate $-\alpha_i$ of the instability waves have revealed that instability takes place in a broad range of frequencies f from about 10 to 360 kHz and at angles of the wave vector orientation ($\chi = \arctan \beta/\alpha$) between $0 \le \chi < 88$ deg (see Fig. 22a in [1]). The highest amplification at the sensor position takes place for waves with a frequency of $f \approx 277$ kHz and $\chi = 0$ deg. This is a 2-D second instability mode. There is also a secondary smaller peak of the growth rate at $f \approx 51$ kHz and $\chi = 60$ deg, corresponding to a 3-D first mode of instability. The frequencies of these two peaks of the amplification rate correlate with the measured maxima of the fluctuation spectrum (see Fig. 14).

Furthermore, the LST eigenfunctions have been calculated; that is, the fluctuations of mass flux, pressure, and temperature across the BL have been performed for waves with parameters that precisely correspond to the positions of the two peaks in growth rate (see Fig. 23 in [1]). It is noteworthy that the distributions found for the mass-flux disturbance $A = |A(y)|$ for waves of both frequencies $f \approx 51$ and 277 kHz (i.e., for the FM and SM instability) are very similar and have a maximum close to the BL outer edge.

A discussion of the other eigenvalues concerning the distribution of the pressure and temperature fluctuation of both instability modes across the BL is also very informative (instructive). The computations show that the first-mode pressure disturbance ($|p| \le 0.1$) is small compared with the nondimensional mass-flux disturbance and is almost constant across the BL. In contrast, for the second mode, pressure perturbations grow in the direction of the surface and reach a maximum of about $|p|_{\max} \approx 0.8$ at the wall. This is much larger than for the first mode. Nondimensional temperature disturbance θ has its absolute maximum in the outer half of the BL for both modes. Although the temperature perturbation of the second mode has an additional secondary local maximum closer to the wall, temperature disturbance of the first mode is monotonously decreasing to the wall.

The second instability mode is commonly considered to be a wave of an acoustic nature, which propagates downstream in the BL such as in the waveguide, whereas the first instability mode is more of a vorticity mode. Fluctuation pressure profiles, not shown here (see Fig. 23 in [1]), confirm this point of view: for the second (acoustical) mode, the pressure disturbance in the BL is much higher than for the first mode.

The wall heat-flux fluctuations measured by the ALTP sensor $\dot{q} = -\lambda \mathrm{d}\theta/\mathrm{d}y$ (where λ is the thermal conductivity coefficient of the gas at the wall $y = 0$) is proportional to the disturbance temperature gradient at the wall $\kappa = |\mathrm{d}\theta/\mathrm{d}y|(y = 0)$. Computations show that this temperature gradient κ for the second mode is much larger than for the first mode. This high wall heat flux for the second mode can be explained by the *compressibility effect*: high pressure fluctuation at the wall produces strong temperature fluctuation close to the wall (because density fluctuations are relatively small at the wall) and therefore a high-temperature gradient is developed at the wall.

According to the LST, instability waves in a cold hypersonic BL of the same amplitude of the mass-flux fluctuation *in* the BL can induce different amplitudes of heat-flux fluctuation at the wall.

Contour plots of the growth rate $-\alpha_i$ and of the wall heat-flux coefficient κ as a function of f and χ have been computed in [1] assuming $\max_{0 \le y < \infty} |A(f, \chi)| = 1$. This means that κ is actually proportional to the wall heat flux induced by waves of the same intensity of the mass-flux perturbation at the maximum. In the range of parameters investigated, there is only one sharp maximum at the parameters *exactly* corresponding to the second instability mode with maximal spatial amplification (see Fig. 22 in [1]).

In the measurements, no spectral analysis over spanwise wave numbers has been performed. For further theoretical analysis, it is therefore necessary to make some assumptions about the dominant contribution to the actual frequency-wave number spectrum of the disturbances in the real flow. One can assume, for example, that for each frequency f, the wave with the angle $\chi = \chi_{\max}$, which corresponds to the maximum amplification rate $\max_{\chi \ge 0}[-\alpha_i(f, \chi)]$, is dominant. For the sake of simplicity, it has been assumed in the present investigation that for $f \ge 225$ kHz, the 2-D waves make the dominant contribution, whereas for $f < 225$ kHz, the 3-D waves defined in the α_i–χ plane along a trajectory of $\max_{0 \le \chi < 90\,\mathrm{deg}}[-\alpha_i]$ and approximated by a straight line (see Fig. 22a of [1]) could give a relevant contribution to the fluctuation.

Figure 15 presents the plot of $\kappa = \kappa(f)$ for the case for pure 2-D modes and along the trajectory $\max[-\alpha_i]$ for 3-D waves. The two curves show that the ratio of wall heat fluxes induced by the instability waves of the same mass-flux amplitude propagating in the BL can reach 1 order of magnitude for the second-mode maximum at $f \approx 270$ kHz in reference to the first mode in the frequency range $50 \le f \le 100$ kHz. This diagram qualitatively explains the discrepancy observed of the ALTP and HW spectra; the absence of the first mode at the ALTP spectra is explained from the standpoint of LST by too-low wall heat-flux fluctuation induced by the instability waves within the relevant first-mode frequency range, which cannot be captured by the limited sensitivity of the sensor.

V. Conclusions

The capability of the YBCO Atomic Layer Thermopile as a new heat-flux gauge in fluid mechanics is depicted by the correlation of its signal with natural flow phenomena. The principle of operation is compared with other categories of established heat-flux measure-

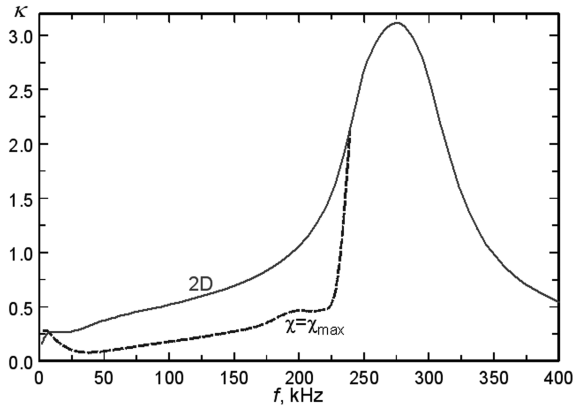

Fig. 15 Fluctuation wall heat flux κ versus frequency f.

ment techniques. Its dynamic properties are studied by the exposure to a diode laser beam with a square wave test as well as by theoretical estimations employing standard techniques.

As a first case of application, the transition process within the unsteady boundary layer of a transient flow developing behind a traveling shock wave is investigated. The signal response shows that the passing of the incident shock over the gauge could be resolved in an interval of 0.35 μs. The successive convective heat-flux rise within less than 1 μs demonstrates that the ALTP gauge has a frequency response of almost 1 MHz. The congruence between frequency response determined experimentally and theoretically is good up to an attenuation of -3 dB, corresponding to a frequency of about 300 kHz. The discrepancy in the results lies in the uncertainty of the assumed film thickness. The theoretical studies also reveal the dependency of the time constant on film thickness and demonstrate the potential of frequency-response enlargement by reducing the ALTP film thickness.

The second experiment presented demonstrates a new possibility for detecting traveling high-frequency instability waves. A second-mode instability is detected in the prestage of the transition process of a conical steady hypersonic boundary layer at Mach 6. For the first time (to the authors' knowledge), comparative measurements are carried out at such a high flow speed and corresponding frequency level by means of a hot wire for mass-flux fluctuations with correlating heat-flux fluctuation measurements at the wall for detecting instability modes. The heat-flux fluctuations detect a kind of instantaneous footprint of these unstable boundary-layer phenomena. Even a first harmonic of the second-mode instability between 430 and 730 kHz could be captured by the ALTP in a frequency range that could not be achieved by the available constant-current anemometer hot-wire system.

Thus, the ALTP sensor also opens up new possibilities for BL stability studies in short-term ground-testing facilities in which higher stagnation enthalpy and hypervelocity are simulated and in which the use of the conventional hot-wire measurement technique is no longer possible.

Acknowledgments

This research was partly supported by the German Research Foundation (DFG) as part of the KN 490/1-1 project. The administrative support by E. Kraemer [Institute of Aerodynamics and Gas Dynamics (IAG)], S. Wagner (IAG, retired), and F. Seiler [French–German Research Institute of Saint-Louis (ISL)] is gratefully acknowledged. We gratefully acknowledge the assistance of B. Sauerwein of the ISL. We greatly appreciate the creation of specific Atomic Layer Thermopile prototypes in cooperation with J. Betz of FORTECH. We thank A. Nolan for technical editing.

References

[1] Knauss, H., Roediger, T., Gaisbauer, U., Kraemer, E., Bountin, D. A., Smorodsky, B. V., Maslov, A.A., Srulijes, J., Seiler, F., "A Novel Sensor for Fast Heat Flux Measurements," AIAA Paper 2006-3637, 2006.

[2] Lengfellner, H., Kremb, G., Schnellbögl, A., Betz, J., Renk, K. F., and Prettl, W., "Giant Voltages upon Surface Heating in Normal YBCO Films Suggesting an Atomic Layer Thermopile," *Applied Physics Letters*, Vol. 60, No. 4, 1992, pp. 501–550. doi:10.1063/1.106613

[3] Renk, K. F., Betz., J., Zeuner, S., Lengfellner, H., and Prettl, W., "Thermopile Effect Due to Laser Radiation Heating in Thin Films of High-TC Materials," *Physica C: Superconductivity and Its Applications (Amsterdam)*, Vols. 235–240, 1994, pp. 37–40. doi:10.1016/0921-4534(94)91308-0

[4] Lengfellner, H., Zeuner, S., Prettl, W., and Renk, K. F., "Thermoelectric Effect in Normal-State YBCO Films," *Europhysics Letters*, Vol. 25, No. 5, 1994, pp. 375–378. doi:10.1209/0295-5075/25/5/011

[5] Mityakov, A. V., Mityakov, V. Y., Sapozhnikov, S. Z., and Chumakov, Y. S., "Application of the Transverse Seebeck Effect to Measurement of Instantaneous Values of a Heat Flux on a Vertical Heated Surface Under Condition of Free-Convection Heat Transfer," *High Temperature*, Vol. 40, No. 4, 2002, pp. 620–625. doi:10.1023/A:1019683617967

[6] Sapozhnikov, S. Z., Mityakov, V. Y., Mityakov, A. V., Petrov, R. L., Grigor'ev, V. V., Bobashev, S. V., Mende, N. P., and Sakharov, V. A., "Heat Flux Measurements on the Inner Walls of a Shock Tube," *Technical Physics Letters*, Vol. 30, No. 1, 2004, pp. 76–77. doi:10.1134/1.1646722

[7] Zahner, T. H., Förg, R., and Lengfellner, H., "Transverse Thermoelectric Response of a Tilted Metallic Multi Layer Structure," *Applied Physics Letters*, Vol. 73, No. 10, Sept. 1998, pp. 1364–1366. doi:10.1063/1.122376

[8] Raphael-Mabel, S., "Design and Calibration of a Novel High Temperature Heat Flux Sensor," M.S. Thesis, Virginia Polytechnic Inst. and State Univ., Blacksburg, VA, Feb. 2005.

[9] Roediger, T., Jenkins, S., Knauss, H., von Wolfersdorf, J., Gaisbauer, U., and Kraemer, E., "Time-Resolved Heat Transfer Measurements on the Tip Wall of a Ribbed Channel Using a Novel Heat Flux Sensor—Part 1: Sensor and Benchmarks," *Journal of Turbomachinery*, Vol. 130, No. 1, Jan. 2008, Paper 011018. doi:10.1115/1.2751141

[10] Knauss, H., Gaisbauer, U., Wagner, S., Buntin, D., Maslov, A., Smorodsky, B., and Betz, J., "Calibration Experiments of a New Active Fast Response Heat Flux Sensor to Measure Total Temperature Fluctuations Part 3," *Proceedings of ICMAR 2002*, Vol. 3, Nonparel Publishing, Novosibirsk, Russia, 2002, pp. 103–113.

[11] Zeuner, S., "Atomlagenthermosäulen in Hochtemperatur-Supraleitern als Schnelle Strahlungsdetektoren," Ph.D. Thesis, Univ. of Regensburg, Regensburg, Bavaria, Germany, 1994 (in German).

[12] Yasuoka, H., Mazaki, H., Terashima, T., and Yoshichika, B., "Optical Absorption Spectra of Single-Crystal $YBa_2Cu_3O_y$ Films," *Physica C: Superconductivity and Its Applications (Amsterdam)*, Vol. 175, Nos. 1–2, 1991, pp. 192–196. doi:10.1016/0921-4534(91)90252-T

[13] Zibold, A., Widder, K., Geserich, H. P., Scherer, T., Marienhoff, P., Neuhaus, M., Jutzi, W., Erb, A., and Müller-Vogt, G., "Optical Anisotropy of $YBa_2Cu_3O_{7-\delta}$ Films on $NdGa_3$ (001) Substrates: A Comparison with Single Domain Crystals," *Applied Physics Letters*, Vol. 61, No. 3, 1992, pp. 345–347. doi:10.1063/1.107932

[14] Zeuner, S., Lengfellner, H., and Prettl, W., "Thermal Boundary Resistance and Diffusility for $YBa_2Cu_3O_{7-d}$ Films," *Physical Review B*, Vol. 51, No. 17, 1995, pp. 11903–11908.

[15] Carslaw, H. S., and Jaeger, J. C., *Conduction of Heat in Solids*, 2nd ed., Oxford Univ., Oxford, 1959.

[16] Olivier, H., "Thin Film Gauges and Coaxial Thermocouples for Measuring Transient Temperatures," Shock Wave Lab. Aachen, Germany, 2003.

[17] Roberts, A. S., Jr., Ortgies, K. R., Gartenberg, E., and Carraway, D. L., "Convective Response of a Wall-Mounted Hot Film Sensor in a Shock Tube," *International Symposium on Non-Steady Fluid Dynamics*, edited by J. A. Miller and D. P. Telionis, American Society of Mechanical Engineers, New York, 1990, pp. 253–258.

[18] Holmberg, D. G., Mukkamala, Y. S., and Diller, T. E., "Shock Tunnel Evaluation of Heat Flux Sensors," AIAA Paper 94-0730, 1994.

[19] Hager, J. M., Langley, L. W., Onishi, S., and Diller, T. E., "Microsensors for High Heat Flux Measurements," *Journal of Thermophysics and Heat Transfer*, Vol. 7, No. 3, 1993, pp. 531–534. doi:10.2514/3.452

[20] Hayashi, M., Sakurai, A., and Aso, S., "Measurement of Heat Transfer Coefficients in Shock Wave-Turbulent Boundary Layer Interaction Regions with a Multi-Layered Thin Film Heat Transfer Gauge," NASA TM-77958, 1986.
[21] Mirels, H., "Laminar Boundary Layer Behind Shock Advancing into Stationary Fluid," NACA TN 3401, 1955.
[22] Davies, W. R., and Bernstein, L., "Heat Transfer and Transition to Turbulence in the Shock-Induced Boundary Layer on a Semi-Infinite flat plate," *Journal of Fluid Mechanics*, Vol. 36, No. 1, 1969, pp. 87–112.
doi:10.1017/S0022112069001534
[23] Mirels, H., "Laminar Boundary Layer Behind a Strong Shock Moving into Air," NASA TN-D 291, 1961.
[24] Weatherstone, R. C., Russo, A. L., Smith, W. E., and Marrone, P. V., "Gasdynamics of a Wave Superheater Facility for Hypersonic Research and Development," U.S. Air Force Office of Scientific Research Rept. TN 59-107, Buffalo, NY, 1959.
[25] Mirels, H., "Shock Tube Test Time Limitation due to Turbulent-Wall Boundary Layer," *AIAA Journal*, Vol. 2, No. 1, 1964, pp. 84–93.
doi:10.2514/3.2218
[26] Oertel, H., *Stoßrohre*, Springer–Verlag Wien, Germany, 1966.
[27] Spence, D. A., and Woods, B. A., "A Review of Theoretical Treatments of Shock-Tube Attenuation," *Journal of Fluid Mechanics*, Vol. 19, 1964, pp. 161–174.
doi:10.1017/S0022112064000623
[28] Hartunian, R. A., Russo, A. L., and Marrone, P. V., "Boundary-Layer Transition and Heat Transfer in Shock Tubes," *Journal of the Aeronautical Sciences*, Vol. 27, No. 8, 1960, pp. 587–594.
[29] Mark, H., and Mirtich, M. J., Jr., "Transition in Shock-Tube Boundary Layers," *Physics of Fluids*, Vol. 5, No. 2, 1962, pp. 251–253.
doi:10.1063/1.1706605
[30] Thompson, W. P., and Emrich, R. J., "Turbulent Spots and Wall Roughness Effects in Shock Tube Boundary Layer Transition," *Physics of Fluids*, Vol. 10, No. 1, 1967, pp. 17–20.
doi:10.1063/1.1761968
[31] Chaney, M. J., and Cook, W. J., "Further Experiments on Shock Tube Wall Boundary-Layer Transition," *AIAA Journal*, Vol. 21, No. 7, 1983, pp. 1046–1048.
doi:10.2514/3.60138
[32] Brun, R., "Comment on 'Further Experiments on Shock-Tube Wall Boundary-Layer Transition," *AIAA Journal*, Vol. 23, No. 8, 1985, pp. 1297–1299.
doi:10.2514/3.9084
[33] Mirels, H., "Turbulent Boundary Layer Behind Constant Velocity Shock Including Wall Blowing Effects," *AIAA Journal*, Vol. 22, No. 8, 1984, pp. 1042–1047.
doi:10.2514/3.8736
[34] Dillon, R. E., and Nagamatsut, H. T., "Heat Transfer and Transition Mechanism on a Shock-Tube Wall," *AIAA Journal*, Vol. 22, No. 11, 1982, pp. 1524–1527.
[35] Cook, W. J., and Feldermann, F. J., "Reduction of Data from Thin Film Heat Transfer Gauges, a Concise Numerical Technique," *AIAA Journal*, Vol. 43, 1996, p. 561.
[36] Srulijes, J., and Seiler, F., "Analytically Obtained Data Compared with Shock Tunnel Heat Flux Measurements at a Conical Body at $M = 6$," French–German Research Inst. of Saint-Louis, Rept. PU 662/2004, Saint-Louis Cedex, France, Nov. 2004.
[37] Mack, L. M., "Boundary Layer Stability Theory," Jet Propulsion Lab., California Inst. of Technology, Rept. 900-277, Rev. A., Pasadena, CA, 1969.
[38] Kendall, J. M., "Wind Tunnel Experiments Relating to Supersonic and Hypersonic Boundary Layer Transition," *AIAA Journal*, Vol. 13, No. 3, 1975, pp. 290–299.
doi:10.2514/3.49694
[39] Demetriades, A., "New Experiments on Hypersonic Boundary Layer Stability Including Wall Temperature Effect," *Proceedings of the Heat Transfer and Fluid Mechanics Institute*, Vol. 26, No. 39, 1978, pp. 39–54.
[40] Stetson, K., Thompson, E., Donaldson, J., and Siler, L., "Laminar Boundary Layer Stability Experiments on a Cone at Mach 8, Part 1: Sharp Cone," AIAA Paper 83-1761, 1983.
[41] Maslov, A. A., Shiplyuk, A. N., Bountin, D. A., and Sidorenko, A. A., "Mach 6 Boundary-Layer Stability Experiments on Sharp and Blunted Cones," *Journal of Spacecraft and Rockets*, Vol. 43, No. 1, 2006, pp. 71–76.
doi:10.2514/1.15246
[42] Anderson, J. D., *Modern Compressible Flow*, McGraw–Hill, New York, 1990.
[43] Dorrance, W. H., *Viscous Hypersonic Flow Theory of Reacting and Hypersonic Boundary Layers*, McGraw–Hill, New York, 1962.
[44] Zhigulev, V. N., and Tumin, A. M., *The Origin of Turbulence*, Science, Novosibirsk, Russia, 1987 (in Russian).
[45] Gaponov, S. A., and Maslov, A. A., *Development of Disturbances in Compressible Flows*, Science, Novosibirsk, Russia, 1980 (in Russian).

G. Palmer
Associate Editor